Applied Acoustics 198 (2022) 108984

Contents lists available at ScienceDirect

Applied Acoustics

journal homepage: www.elsevier.com/locate/apacoust

Effects of urea–formaldehyde and polyvinyl acetate adhesive on sound absorption coefficient and sound transmission loss of palmyra palm fruit fiber composites

Purintorn Chanlert [a,*], Sukrutai Tongyoo [b], Chintaporn Rordrak [b]

[a] Faculty of Science and Technology, Songkhla Rajabhat University, Kaorupchang, Muang, Songkhla 90000, Thailand
[b] Faculty of Education, Songkhla Rajabhat University, Kaorupchang, Muang, Songkhla 90000, Thailand

ARTICLE INFO

Article history:
Received 15 February 2022
Received in revised form 28 June 2022
Accepted 13 August 2022

Keywords:
Palmyra palm fruit fiber
Urea–formaldehyde
Polyvinyl acetate
Sound absorption coefficient
Sound transmission loss

ABSTRACT

Composite materials made from palmyra palm fruit fiber (PPFF) were formed using urea–formaldehyde (UF) and polyvinyl acetate (PVAc). We prepared two sets of five different cylindrical samples with varying PPFF contents. The PPFF composites' normal-incident sound absorption coefficient (SAC) and transmission loss (TL) were measured by using the impedance tube method. The sample with higher PPFF content shows a lower SAC spectrum. It is the opposite for the TL, where a sample with high PPFF content demonstrates a higher TL spectrum. We conducted the least-square fitting method on the experimental SAC and TL spectra utilizing the Johnson-Champoux-Allard (JCA) equivalent fluid model. Non-acoustic parameters were acquired from the fitting. The optimized porosity (ϕ), viscous characteristic length (Λ), and thermal characteristic length (Λ') are inversely proportional to the PPFF content. The airflow resistivity (σ) and tortuosity (α_∞), on the other hand, demonstrate a direct correlation with the PPFF content. Even though the UF samples have an average density of 14.7 % higher than the PVAc samples, their σ, Λ', and α_∞ are just 7.7 %, 4.5 %, and 0.39 % higher than PVAc samples. On the other hand, PVAc samples show higher average Λ and ϕ of 1.4 % and 0.73 %, respectively. The optimized porosity values obtained from the JCA model (ϕ_{JCA}) are coherent with ones from the direct estimation method assuming adhesive-coated fiber (ϕ_{fa}). It can be concluded that the adhesive's quantity and density contribute to the composites' porosity value, ultimately affecting material acoustic properties. Researchers can control and predict how the SAC and TL of fibrous sound absorbers would behave by varying the quantity and density of an adhesive.

1. Introduction

Noise is an unpleasant or distracting sound, including traffic, building sites, factories, and even noise inside a household. There are two sorts of noise to consider in most cases. The first is internal noise, such as sound reverberation. It occurs when a sound wave reflects in a closed space with multiple reflecting bodies, causing sound perception to be distracted. The second is noises generated externally, such as those from a busy street or a construction site, propagating into households. Two types of noises require different ratings. For the internally generated noise, the sound absorption coefficient (SAC) is a rating of how much sound material can absorb (on a scale of 0 to 1). On the other hand, for the externally generated noise, the sound transmission loss (TL) is a number rating of how efficiently a material attenuates airborne sound.

Glass wool and rock wool have been in the industry for a long time [1–3]. Not only are they used as solutions for reducing reverberation sound, but they are also used in sound insulating in the form of multilayer structures. However, both materials have severe effects on the environment since they are difficult to get eradicated [4]. Furthermore, the production and application of these materials deteriorate the health of people who have associated [5].

Alternative sound absorbers were required since substitutions were necessary for the glass and rock wools. In 2002, Koizumi et al. [6] investigated the sound absorption performance of bamboo fiber materials by varying parameters, including panel thickness, apparent density, and fiber diameter. Bamboo fiber exhibits sound absorption property equivalent to glass wool. Their work has motivated researchers to investigate the potential of natural acoustic materials further. In 2003, Yang et al. [7] examined the

* Corresponding author.
E-mail address: purintorn.ch@skru.ac.th (P. Chanlert).

https://doi.org/10.1016/j.apacoust.2022.108984
0003-682X/

sound absorption property of rice straw-wood composites. The composites with a specific gravity of 0.4 show normal-incident sound absorption coefficient (SAC) values greater than 0.6 at a frequency above 2000 Hz. From the study of Zulkifli et al. [8], and Hossein et al. [9], coconut coir fiber also shows excellent sound-absorbing properties. The coir panel with 30 mm thickness demonstrates an average SAC greater than 0.7 at frequencies above 600 Hz. By combing the coir fiber and the perforated plate as multilayer absorbers, sound absorption seems to improve at low frequency. On the other hand, the combination reduces the value at the medium frequency. In 2012, Kang et al. [10] proposed the study where rice hull-sawdust composite board showed higher SAC than the commercial gypsum board. For the sample with 400 kg/m^3 density, the SAC is around 0.40–0.55 at the frequency over 1000 Hz.

Recently, natural materials, especially those from agricultural leftovers, attracted interest from researchers. In 2020, Taban et al. [11] reported sound absorption behavior of the composites made from kenaf fiber. The noise reduction coefficient (NRC) of the sample with 45 mm thickness is 0.65. They used Delany-Bazley (D-B) model [12] and the best-fit inverse law [13] in describing sound absorption behavior in a mathematical approach. Similar research extended towards fibrogranular composites made from kenaf fiber and rice husk granule [14], chrome shave and coffee silver skin [15], date palm fiber [16], and sugarcane bagasse [17]. According to these investigations, natural materials have a lot of potentials to be used as sound-absorbing materials.

The palmyra palm (*Borassus flabellifer* L.) is a type of palm plant native to South and Southeast Asia, particularly in dry, coastal, and low-altitude areas. The husk color of ripe palm fruit is purplish-black, while the mesocarp pulp around the seeds is fibrous, yellowish, and oily [18]. The palmyra palm is commonly used for fruit and juice consumption [19]. However, the leftover mesocarp is typically discarded. Therefore, it is intriguing to see what else it could perform after recycling since the act of waste recycling can have economic, social, and environmental benefits. Due to its fibrous characteristics, it can be used as a substitution for rock/glass wool as an acoustic absorber.

In this study, we manufactured the sound absorbers made from palmyra palm fruit fiber (PPFF) binding by two different adhesives; urea–formaldehyde (UF) and polyvinyl acetate (PVAc). The samples' normal-incident sound absorption coefficient (SAC) and transmission loss (TL) were measured and reported. Five essential non-acoustic parameters, including the airflow resistivity (σ), porosity(ϕ), tortuosity(α_∞), viscous characteristic length (Λ), and thermal characteristic length (Λ') were optimized from the least-square fitting of the Johnson-Champoux-Allar (JCA) equivalent fluid model [20,21]. The optimized parameters were analyzed to reveal the effects of adhesive on the material's acoustic properties.

This article is ordered into five sections; the following Section 2 focuses on the preparation of the samples and the measurement of material acoustic properties. The experimental results are presented and explained in Section 3. In Section 4, experimental results are interpreted and discussed. Finally, Section 5 summarizes the main findings of this study.

Fig. 1. (a) Fresh palmyra palm fruit fiber (PPFF) where juice is not yet extracted (b) dried PPFF after juice extraction and convection drying.

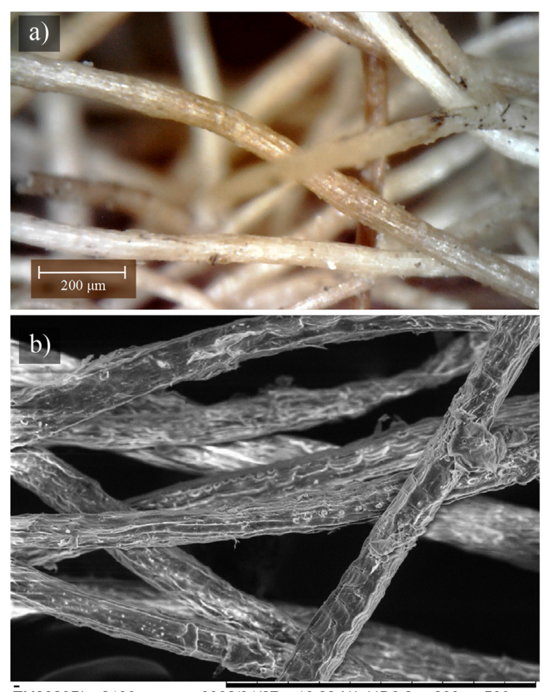

Fig. 2. a) Optical microscopic image and b) scanning electron microscopic image (SEM) of palmyra palm fruit fiber.

2. Materials and methods

2.1. Sample preparation

In this study, we collected the Palmyra palm fruit fiber (PPFF) from the dried palm fruits as demonstrated in Fig. 1. The fiber length was controlled by cutting fiber to be around 50 mm. According to Fig. 2, the average diameter of fibers is around 60 $\pm$ 18 μm obtained from SEM images using ImageJ software [22]. Palm fiber was dried in an air-circulating oven at 60 °C for 120 min. Commercial urea–formaldehyde (UF) adhesive powder (Bosny brand, England) and polyvinyl acetate copolymer emulsion (PVAc) adhesive (TOA brand, Thailand) were utilized in this study. The density of the dried UF and PVAc adhesives were measured to be around 1282 and 1190 kg/m^3 for UF and PVAc adhesives, respectively. The UF adhesive powder was dissolved in water with a 2:1 adhesive to water ratio. We prepared the cylindrical specimens with 29.0 mm diameter and 40.0 mm thickness using the stainless steel mold. The PPFF contents in the test specimens were varied by 4.0, 4.5, 5.0, 5.5, and 6.0 g. Meanwhile, the UF adhesive and water content were fixed at 3.8 g and 1.9 g, respectively. In contrast to the UF adhesive, the commercial PVAc was initially polymerized and already in water emulsion form. From our observation, 8.0 g of the PVAc emulsion is reduced to approximately 1.9 g after drying. The Variation of PPFF content is the same as in UF samples, while the PVAc emulsion adhesive was fixed at 8.0 g (1.9 g dried weight). After properly combining the components, we put the wet mixture inside the mold.

The proper load was placed above the mold edge during preparation to keep the wet composites from overflowing. Next, we put the wet specimens in an air-circulating oven set to 60 °C for 120 min to remove the excess moisture. Then, all specimens shown in Fig. 3 were stored in dried sample storage for five days. After drying, the samples' weight, surface density, and bulk density were measured and displayed in Table 1.

2.2. Sound absorption measurement

The normal-incident sound absorption coefficients (SAC) of materials were measured using the two-microphone impedance tube explicitly designed according to ASTM E1050-98 [23] and ISO 10534–2 standard [24]. It was designed as a one-size impedance tube where a sample with only one diameter size is required in the measurement [25]. The internal tube diameter of the cylindrical-shaped impedance tube is 29.0 mm, and made of stainless steel. Two 1/4-inch measurement microphones (GRAS 40PP) are hermetically sealed against the tube's wall. The first and second microphones have a distance of 20 mm, resulting in measurable results at frequencies between 100 and 5,000 Hz [23] [24]. A generic full-range speaker is set at the end of the impedance tube to provide a broadband sound signal inside the tube. The length of 100 cm, the distance between the sound source and the first microphone, is considered sufficient for sound waves to become normal-incident while reaching the sample's surface. The cylinder-shaped sample was firmly inserted into the sample holder, which was attached to the tube's opposite end. Next to the sample, an echoic hard backing plate was placed to prevent sound waves from leaking out. Fig. 4 shows the diagram of the impedance tube. Signals from both microphones are acquired using the data acquisition device (NI-9230 DAQ, National Instrument) as shown in Fig. 5. PYTHON's data acquisition module examined the transfer function (H_{12}) of the signals between two microphones. Equations below explain the calculation of the sound absorption coefficient using the transfer function H_{12}:

$$R = \frac{H_{12} - e^{-jk_0 s}}{e^{jk_0 s} - H_{12}} e^{2jk_0 x_1} \tag{1}$$

$$\mathrm{SAC} = 1 - |R|^2 \tag{2}$$

where R is the complex sound reflection coefficient. j is the complex number $\sqrt{-1}$. k_0 is the wavenumber. x_1 is the distance between the first microphone (Mic 1) and the sample. s is the distance between two microphones, and SAC is the normal-incident sound absorption coefficient, which ranges from 0 to 1. Typically, the SAC is reported as a spectrum since the incident wave frequencies substantially influence the sound absorption coefficient.

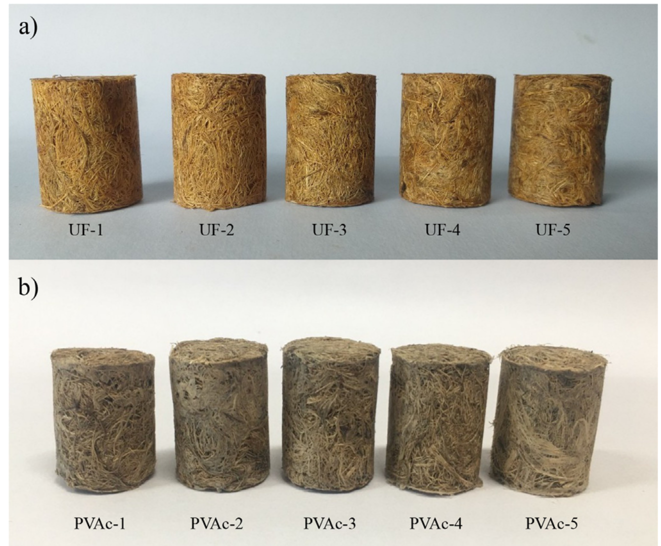

Fig. 3. (a) Samples with PPFF and urea formaldehyde (UF) adhesive (b) Samples with PPFF and polyvinyl acetate (PVAc) adhesive.

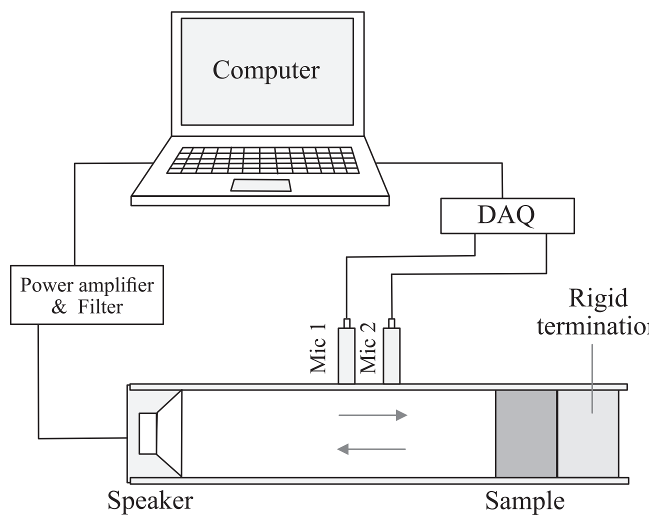

Fig. 4. Impedance tube diagram for sound absorption coefficient (SAC) measurement (two microphone method) according to ASTM E1050-98 [23] and ISO 10534-2 [24].

Table 1
UF and PVAc sample information.

Sample name	PPFF content - m_f (g)	Dried adhesive content - m_a (g)	Dried sample mass (g)	Surface density (kg/m^2)	Bulk density (kg/m^3)
UF-1	4.0	3.8	6.4	9.7	247.6
UF-2	4.5	3.8	7.4	11.2	276.7
UF-3	5.0	3.8	7.6	11.5	281.1
UF-4	5.5	3.8	8.6	13.0	310.2
UF-5	6.0	3.8	9.0	13.6	325.2
PVAc-1	4.0	1.9	5.8	8.8	230.5
PVAc-2	4.5	1.9	6.2	9.4	231.7
PVAc-3	5.0	1.9	6.3	9.5	235.5
PVAc-4	5.5	1.9	6.8	10.3	248.8
PVAc-5	6.0	1.9	7.7	11.7	282.7

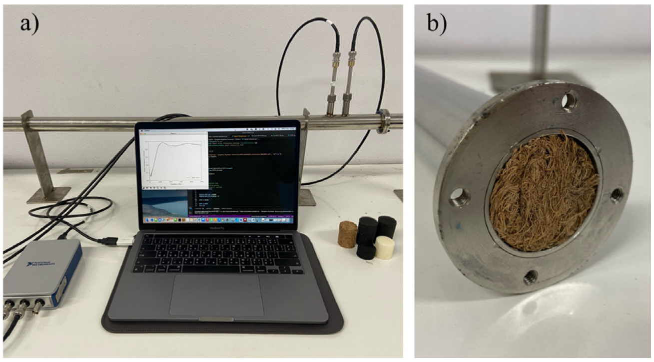

Fig. 5. a) Impedance tube instrument b) cylindrical sample specimen inside the sample holder of the impedance tube.

2.3. Transmission loss measurement

Transmission loss (TL) defines how efficiently an acoustic panel can attenuate the amplitude of sound waves traveling from one side to the other. The value of TL is measured in decibels (dB) reduction. The four-microphone impedance tube is used to measure the normal-incident TL using the transfer matrix method based on the ASTME2611 standard [26]. The measurement configuration is similar to that of the normal-incident SAC, except that there are four microphone positions. The sample specimen is placed between the second and third microphone, as displayed in Fig. 6. The microphones are placed at four positions to measure the acoustic pressure (p) and particle velocity (u). ASTME2611 standard requires two measurements using two different terminations (Termination a and b). Therefore, the transfer matrix (T_n) can be estimated as:

$$T_{11} = \frac{p_{0a}u_{da} - p_{0b}u_{da}}{p_{da}u_{db} - p_{db}u_{da}}, \quad T_{12} = \frac{p_{0b}p_{da} - p_{0a}p_{db}}{p_{da}u_{db} - p_{db}u_{da}}$$
$$T_{21} = \frac{u_{0a}u_{db} - u_{0b}u_{da}}{p_{da}u_{db} - p_{db}u_{da}}, \quad T_{22} = \frac{p_{da}u_{0b} - p_{db}u_{0a}}{p_{da}u_{db} - p_{db}u_{da}} \tag{3}$$
$$T_n = \begin{bmatrix} T_{11} & T_{12} \\ T_{21} & T_{22} \end{bmatrix}$$

where T_{11}, T_{12}, T_{21} and T_{22} are four components of 2 x 2 transfer matrix. p_{0a}, p_{0b}, p_{da} and p_{db} are acoustic pressures at position $x = 0$ and $x = d$. u_{0a}, u_{0b}, u_{da} and u_{db} are particle velocities at $x = 0$ and $x = d$. Thus, the sound transmission coefficient and normal-incident transmission loss (TL) can be determined as [26]:

$$t = \frac{2e^{jk_0 d}}{T_{11} + (T_{12}/\rho c) + \rho c T_{21} + T_{22}} \tag{4}$$

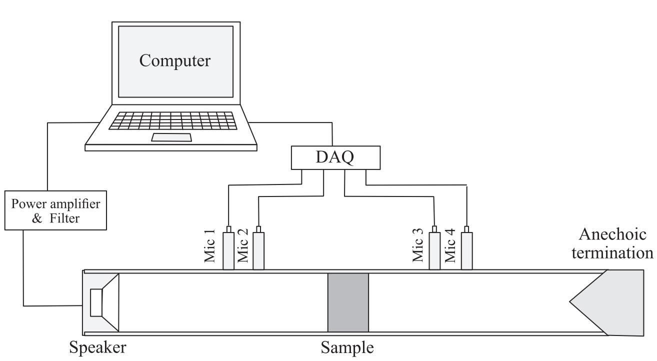

Fig. 6. The impedance tube diagram of the transmission loss (TL) measurement (four microphone method) according to ASTME2611 [26].

$$\mathrm{TL} = 20\log_{10}\left|\frac{1}{t}\right| \tag{5}$$

where t is the sound transmission coefficient. d is the sample thickness. ρ is the static air density, and c is the sound velocity. In this study, the measurements have been conducted using frequencies ranging from 100 to 5000 Hz.

2.4. Least-square fitting and Johnson-Champoux-Allard (JCA) equivalent fluid model

To optimize the acoustic characteristics of porous absorbers, the relationship between non-acoustic and acoustic parameters must be studied. Several acoustic models describe sound propagation inside porous materials considering different morphological parameters [20,21,27,28]. According to the work of Johnson et al. [20], and Allard and Champoux [21], the semi-phenomenological Johnson-Champoux-Allard (JCA) equivalent fluid model has been proposed. The non-acoustical parameters include static airflow resistivity (σ), porosity(ϕ), tortuosity(α_∞), viscous characteristic length (Λ), and thermal characteristic length (Λ'), are used widely to describe the propagation of sound wave inside porous materials. According to the equivalent fluid approach of the JCA model [29–33], the equivalent dynamic density (ρ_{eq}) and the equivalent dynamic bulk modulus of the air (K_{eq}) inside rigid-frame materials containing air-filled parallel cylindrical pores can be described as functions of angular frequency (ω) as follows:

$$\rho_{eq}(\omega) = \frac{\alpha_\infty \rho_0}{\phi}\left[1 + \frac{\sigma\phi}{j\omega\rho_0\alpha_\infty}\left(1 + \frac{4j{\alpha_\infty}^2\eta\omega\rho_0}{(\sigma\Lambda\phi)^2}\right)^{1/2}\right] \tag{6}$$

$$K_{eq}(\omega) = \frac{\gamma p_0}{\phi}\left(\gamma - (\gamma - 1)\left[1 + \frac{8\eta}{j\Lambda'^2\omega\rho_0 N_{pr}}\left(1 + \frac{j\rho_0 N_{pr}\Lambda'^2\omega}{16\eta}\right)^{1/2}\right]^{-1}\right)^{-1} \tag{7}$$

where γ is the specific heat ratio of the air. η is the dynamic viscosity of the air. p_0 is the atmospheric pressure, and N_{pr} is Prandtl number. In this study, $\gamma = 1.4, \eta = 1.85 \times 10^{-5}, p_0 = 1.0132 \times 10^5$ N/m^2, and $N_{pr} = 0.702$, respectively [21].

Thus, the characteristic wave number $k_c(\omega)$ and the characteristic impedance $Z_c(\omega)$ can be determined by:

$$k_c(\omega) = \omega\sqrt{\frac{\rho_{eq}(\omega)}{K_{eq}(\omega)}} \tag{8}$$

$$Z_c(\omega) = \sqrt{\rho_{eq}(\omega)K_{eq}(\omega)} \tag{9}$$

The surface acoustic impedance ($Z_s(\omega)$) at normal incidence for hard-backed materials with the thickness of d can be estimated using:

$$Z_s(\omega) = -jZ_c\cot(k_c d) \tag{10}$$

Thus, sound absorption coefficient (SAC) at normal incidence can be determined by:

$$\mathrm{SAC} = 1 - \left|\frac{Z_s - \rho_0 c_0}{Z_s + \rho_0 c_0}\right|^2 \tag{11}$$

where c_0 is the sound speed in the air.

In the case of porous material, the normal-incident transmission loss ($\mathrm{TL}(\omega)$) can also be determined using the transfer matrix method [29,34,33]. According to Liu et al. [35], the transfer matrix (T_n) of the porous materials can be described as:

$$T_n = \begin{bmatrix} \cos(k_c d) & jZ_c \sin(k_c d) \\ j \sin(k_c d)/Z_c & \cos(k_c d) \end{bmatrix} \quad (12)$$

The normal-incident transmission loss (TL) can be estimated according to the study of Luu et al. [34] as:

$$\mathrm{TL} = 20\log_{10}\left|\cos(k_c d) + \frac{j\left(Z_c + \frac{1}{Z_c}\right)}{2\rho_0 c_0}\sin(k_c d)\right| \quad (13)$$

The least-square method involves minimizing the sum of the squares of the residuals of the data points from the curve to obtain the curve or line that best fits a set of points. In this study, the least-square method optimizes the five non-acoustic parameters ($\sigma, \phi, \alpha_\infty, \Lambda$, and Λ') within the JCA model (Eq. (11) and (13)) to make curves that best fit the experimental SAC and TL. We used the non-linear least-square optimization method (LMFIT) for PYTHON [36]. However, Optimizing all parameters as independent variables sometimes provides out-of-range results. By applying parameter conditioning, the fitting becomes achievable and reasonable. In this study. we treated ϕ, Λ, and Λ' as independent parameters. On the other hand, σ and α_∞ were treated as dependent parameters. The conditioning was conducted according to Eq. 14 and 16.

The airflow resistivity (σ) can be conditioned as the function of porosity as described by the Carman-Kozen model [37]. The equation for estimating the σ of the fibrous materials as introduced by Pelegrinis et al. [38] is as follows:

$$\sigma\ (\phi) = \frac{180\eta(1-\phi)^2}{d_{\mathrm{mix}}^2\phi^3} \quad (14)$$

where d_{mix} is the diameter of the adhesive-coated fiber. For the fiber-adhesive sound absorber, the actual fiber diameter can be estimated using this equation [38]:

$$d_{\mathrm{mix}}\ (\phi) = d_f + (d_f\phi) \quad (15)$$

where d_f is the average diameter of the PPFF. For the tortuosity (α_∞), it is conditioned using the Berryman's formula [39] as follows:

$$\alpha_\infty\ (\phi) = 1 + \frac{1-\phi}{2\phi} \quad (16)$$

SAC (Eq. 11) and TL (Eq. 13) derived from the JCA model will be used in the least-square fitting method on the experimental SAC and TL. Finally, the discussion section will describe the curve-fitting results and the optimized non-acoustic parameters of all PPFF: adhesive composites.

3. Results

This section discusses the measurement of general sample information and acoustic properties, including sound absorption coefficient (SAC) and transmission loss (TL), according to designed experiments.

3.1. General information of the samples

We manufactured samples with ten formulas from the UF and PVAc adhesive. The numbers at the end of the sample name reflect the PPFF contents. PPFF contents of 4.0, 4.5, 5.0, 5.5, and 6.0 g are labeled by the numbers 1, 2, 3, 4, and 5, respectively. The general information, including sample name, PPFF content (m_f), dried adhesive content (m_a), dried sample mass, surface density, and bulk density, is explained in Table 1.

Samples with higher PPFF contents have higher surface and bulk density. Generally, UF samples have more elevated surface and bulk density than PVAc samples because the amount of PVAc in the samples after drying (approximately 1.9 g) is lower than UF adhesive (3.8 g). Therefore, UF samples generally have a higher average bulk density than PVAc samples by about 14.7 %.

3.2. Sound absorption coefficient spectra

The normal-incident sound absorption coefficient (SAC) is portrayed as frequency dependence. The frequency range is from 100 Hz to 5000 Hz due to the instrumental limitations of the impedance tube [25]. Fig. 7 displays the SAC spectra of UF-1 to UF-5. Since all UF samples possess the porous absorber characteristic, SAC is low at low frequencies and becomes higher while increasing the frequency [13–16]. The SAC generally becomes virtually steady once it reaches saturation [16,40]. By increasing the PPFF content, the SAC spectra of the samples become lower. It suggests that the PPFF content is vital in determining the SAC. The noise reduction coefficient (NRC) provides a good and straightforward estimation of how effectively the particular material can absorb noise. The NRC can be estimated by averaging the values of SAC at the frequencies of 250, 500, 1000, and 2000 Hz [41]. These values encompass the fundamental frequencies and first few overtones of typical human speech. This study assumed that most PPFF samples become saturated at around 1000 Hz. Sound absorption at saturation (α_{sat}) is calculated by averaging all SAC values at the octave frequencies from 1000 to 5000 Hz. The values of NRC and α_{sat} are described in Table 2.

According to Table 2, UF-1 displays the highest SAC spectra among all UF samples. It is the same for PVAc samples as presented in Fig. 8, where PVAc-1 shows the highest SAC spectra. The NRC, which represents average sound absorption at the frequency of 250–2000 Hz, ranges from 0.54–0.62 for UF samples and 0.45–0.63 for PVAc samples, as displayed in Table 2. Besides PVAc-2 and PVAc-5, all PVAc samples show higher NRC than UF samples with the same PPFF contents. The average NRC of PVAc samples is simply 0.68 % higher than UF samples.

UF-1 also shows the highest α_{sat} (0.92) among UF samples. It is the same for PVAc-1, where α_{sat} is the highest (0.91) among all PVAc samples. For other UF and PVAc samples, the α_{sat} becomes lower with higher PPFF content. α_{sat} between UF and PVAc samples with the same PPFF content are not remarkably different. However, the exception is for UF-5 and PVAc-5, where the α_{sat} is diverse.

Some UF and PVAc samples possess similar values of sample bulk density (UF-1 and PVAc-4, and UF-3 and PVAc-5); the SAC spectra between these samples are different. It suggests that density alone does not determine a material's SAC. More analysis is

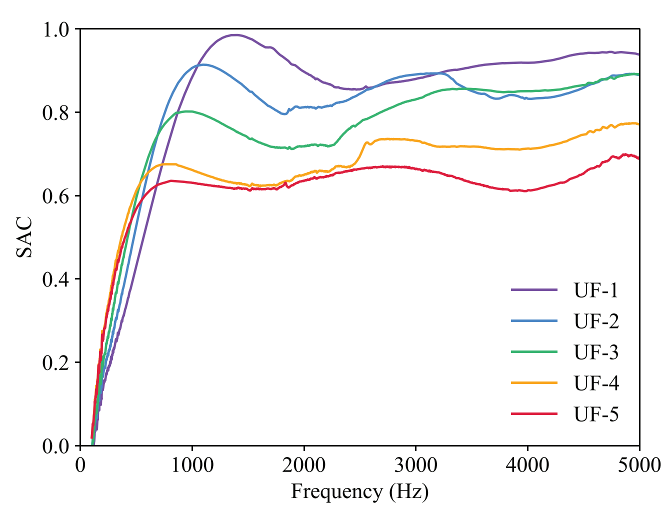

Fig. 7. Normal-incident sound absorption coefficient (SAC) spectra of UF samples.

Table 2
Noise reduction coefficient (NRC), sound absorption at saturation (α_{sat}), TL at 5000 Hz (TL_{5000}), and TL increasing rate (TL_{rate})

Sample	NRC	α_{sat}	TL_{5000} (dB)	TL_{rate} (dB/kHz)
UF-1	0.60	0.92	16.0	1.9
UF-2	0.62	0.86	18.5	2.6
UF-3	0.59	0.80	20.8	2.6
UF-4	0.56	0.68	29.3	3.7
UF-5	0.54	0.64	36.6	4.6
PVAc-1	0.63	0.91	17.4	1.9
PVAc-2	0.60	0.86	18.4	2.3
PVAc-3	0.63	0.79	20.3	2.7
PVAc-4	0.62	0.78	24.4	3.6
PVAc-5	0.45	0.42	37.8	4.2

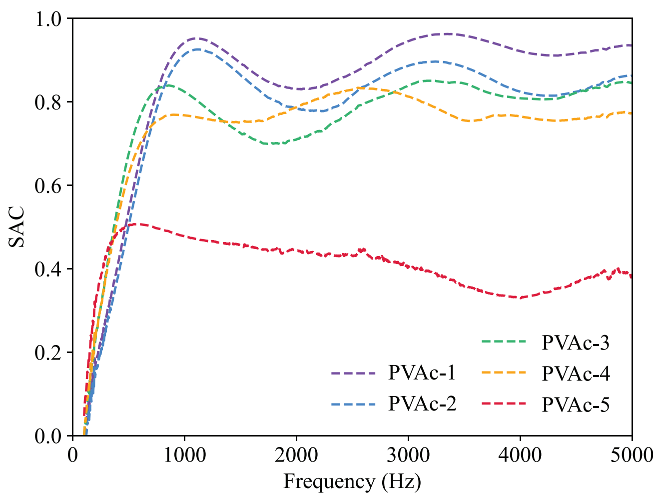

Fig. 8. Normal-incident sound absorption coefficient (SAC) spectra of PVAc samples.

necessary to explain the acoustic characteristics of PPFF composites made from UF and PVAc samples. In this study, the Johnson-Champoux-Allard (JCA) equivalent fluid model was used to describe how non-acoustic parameters, including flow resistivity (σ), porosity(ϕ), tortuosity(α_∞), viscous characteristic length (Λ) and thermal characteristic length (Λ'), contribute to the characteristics of SAC spectra. We use the least-square fitting of the JCA model on the experimental SAC spectra to obtain all mentioned parameters. The transmission loss (TL) spectrum of the same sample is necessary for more accurate parameter optimization. The result of the TL spectra will be presented and described in the following subsection.

3.3. Transmission loss spectra

According to ASTME2611 standard [26], transmission loss (TL) spectra were measured using the four-microphone impedance tube method. The TL spectra of UF and PVAc samples are displayed in Fig. 9 and 10, respectively. Fig. 9 shows the TL spectra of UF-1, UF-2, UF-3, UF-4, and UF-5. In the same way, Fig. 10 displays the TL spectra of PVAc-1, PVAc-2, PVAc-3, PVAc-4, and PVAc-5. The characteristics of the TL spectra are similar for all samples. At low frequency, the TL is controlled by material stiffness (stiffness controlled region) [42] resulting in the drop of TL while frequency increases. After that, the dimension constraints of the impedance tube wall affect the TL behavior resulting in resonance (resonance region) [43]. Then, the TL increases while the frequency rises because the mass of the sample per unit area (sample surface density) plays a significant role (mass controlled region) [43].

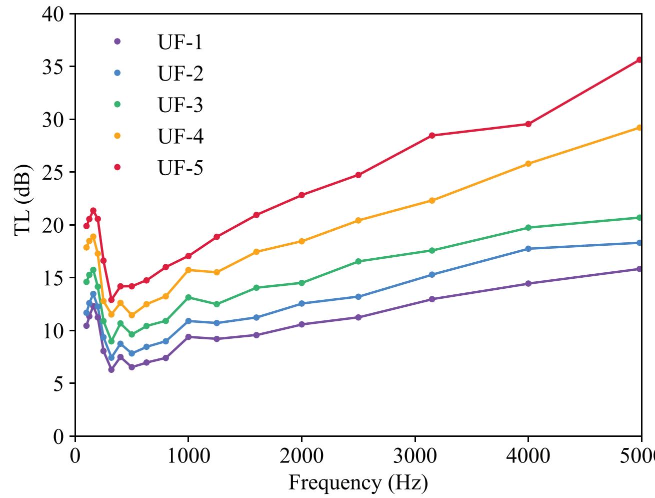

Fig. 9. Normal-incident transmission loss (TL) spectra of UF samples.

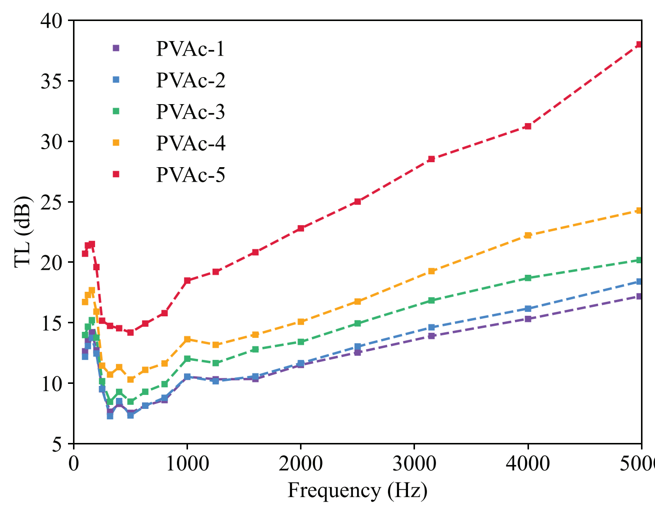

Fig. 10. Normal-incident transmission loss (TL) spectra of PVAc samples.

From Fig. 9 and 10, the spectra show the characteristic of the region, including the stiffness (< 500 Hz), resonance (500–1000 Hz), and mass controlled (>1000 Hz) regions. The appearances of the TL curves are similar for most samples, especially the stiffness and resonance regions, even though they are at different offsets. The values of TL at 5000 Hz (TL_{5000}) of all samples are explained in Table 2. It shows that the values of TL_{5000} are directly variable with the PPFF content. The highest TL_{5000} is 36.6 (UF-5) and 37.8 dB (PVAc-5) for UF and PVAc samples, respectively. UF samples collectively have higher TL_{5000} than PVAc samples since their average TL_{5000} is higher than those from PVAc by 2.4 %.

The TL spectra at the mass control region are almost linear with positive slopes. With higher PPFF content, the samples show higher slopes. The slopes of the TL spectra along the mass control region for UF and PVAc samples are approximately 1.9–4.6 dB/kHz and 1.9–4.2 dB/kHz, respectively. The change of slope is in direct variation with the PPFF content, while the variation due to adhesive type (UF and PVAc) is not significant.

The following section will emphasize the utilization of the least-square fitting on experimental SAC and TL spectra using the JCA model. Non-acoustic parameters obtained from the fitting will be discussed and analyzed.

4. Discussion

4.1. Results of least-square fitting

Fig. 11 and 12 show the least-square fitting of the experimental SAC and the TL using the JCA model. The average of the absolute differences ($\overline{\Delta}_{abs(SAC)}, \overline{\Delta}_{abs(TL)}$) between the experiment and the JCA model are presented in Table 3.

For UF samples, as displayed in Fig. 11, the fittings are mostly in good agreement with the experimental results. From Fig. 11(e), the fitting result of the UF-5 sample shows the highest disagreement between the experimental and theoretical values. $\overline{\Delta}_{abs(SAC)}$ and $\overline{\Delta}_{abs(TL)}$ of UF-5 are 0.046 and 1.152 dB, respectively.

For PVAc samples, as shown in Fig. 12, the experimental and theoretical values are also in decent agreement for most samples. However, the difference is considerably explicit in the case of the PVAc-5, especially the SAC fitting. As displayed in Fig. 12(e), the fitting of the SAC result is in agreement with the frequency below 1000 Hz. However, at a higher frequency, they are explicitly different. $\overline{\Delta}_{abs(SAC)}$ of PVAc-5 is 0.200 which is 5–8 times larger than average $\overline{\Delta}_{abs(SAC)}$ of other PVAc samples. On the other hand, the fitting of the TL spectrum is in good agreement for the PVAc-5 with the $\overline{\Delta}_{abs(TL)}$ of 0.572.

Next, the non-acoustic parameters obtained from the fittings will be discussed and analyzed. The acquired parameters are denoted in Table 4.

4.2. Analysis of the optimized non-acoustic parameters

Five non-acoustic parameters, obtained from the least-square fitting of the experimental results and JCA model, are presented in Table 4. The development of each parameter toward PPFF content is emphasized in Fig. 13.

The airflow resistivity (σ) and tortuosity (α_∞) are the dependent parameters where the values of σ and α_∞ are corresponding to the value of ϕ as explained in Eq. 14 and 16, respectively. Referred to Fig. 13(a) and (c), both σ and α_∞ shows direct variation with the PPFF content. However, the changes between samples are more exponential-liked in the case of σ than α_∞. The average airflow resistivity of UF samples is higher than PVAc samples by 7.7 %. In the same way, their average tortuosity is around 0.39 % higher than the PVAc samples. They correspond with graphs illustrated in Fig. 13. It is reasonable since materials with less porous structure should exhibit higher flow resistance and tortuosity than those with higher porosity.

The independent variables, including viscous characteristic length (Λ) and thermal characteristic length (Λ'), also demonstrate inverse variation with the PPFF content, as demonstrated in Fig. 13. From Fig. 13(d) and (e), it is difficult to conclude which UF or PVAc samples individually exhibit higher Λ and Λ'. Considering their average values, the average Λ of PVAc samples is around 1.4 % higher than the UF samples. On the other hand, UF samples exhibit a higher average Λ' than PVAc by approximately 4.5 %.

Generally, Λ' is always larger or equal to Λ. It is because Λ is related to the width of the interconnection of the pore network where viscous dissipation occurs, while Λ' describes the bigger pore size where the thermal dissipation of sound energy is pronounced [44,45]. Allard and Champoux [21] proposed the relationship between the viscous and thermal characteristic length of the fibrous sound absorber. From their investigation, the thermal characteristic length should be around two times larger than the viscous characteristic length ($\Lambda' = 2\Lambda$) when the flow direction is perpendicular to the fiber orientation [46]. According to the simulation by Luu et al. [34], fibrous materials demonstrate Λ' approximately 1–2 times higher than the value of Λ. In our study, the average values of Λ'/Λ are about 2.0 and 2.1 for UF and PVAc samples, respectively, which are consistent with the previous studies.

According to Fig. 13(b), the porosity (ϕ), which is also an independent fitting parameter, shows inverse variation with the PPFF content. The average porosity of PVAc samples is approximately 0.73 % higher than UF samples. The in-depth investigation of porosity will be discussed in the following subsection.

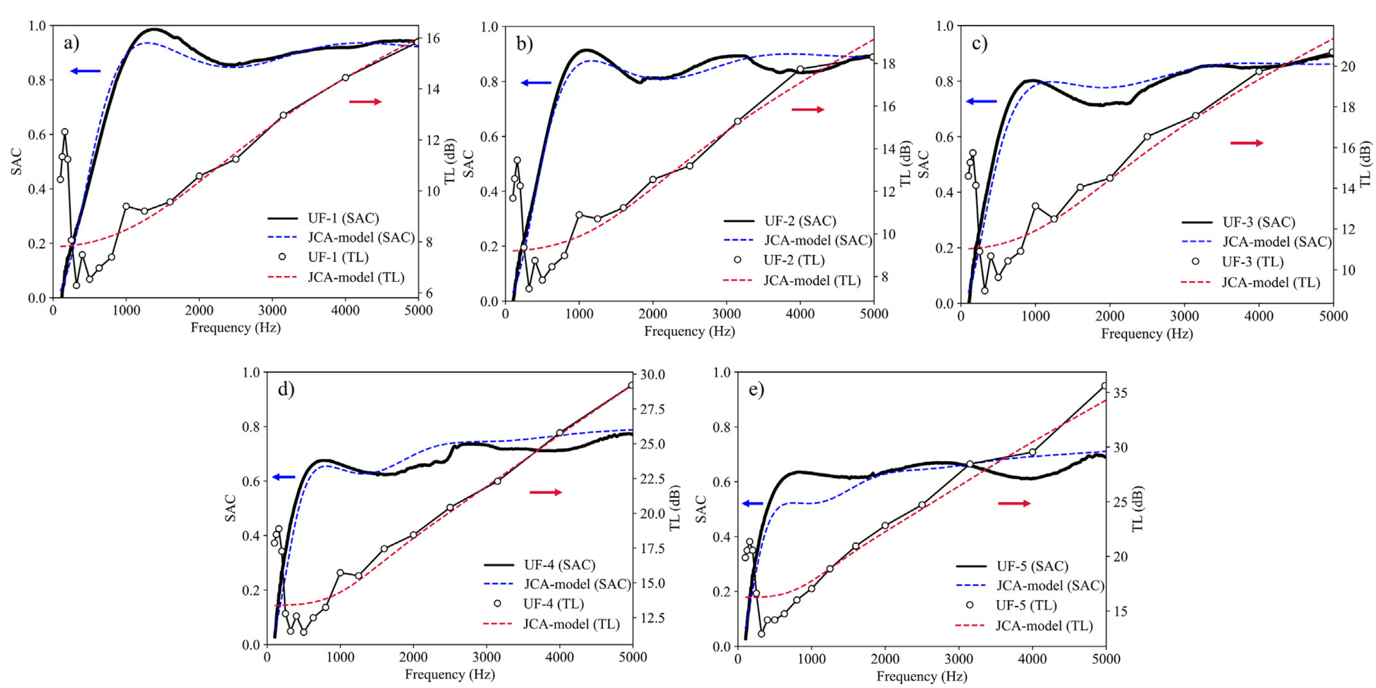

Fig. 11. The experimental sound absorption coefficient (black solid line) and transmission loss (black opened circle) spectra and the least-square fitting of Johnson-Champoux-Allard (JCA) equivalent fluid model (blue and red dashed line for SAC and TL, respectively) a) UF-1 b) UF-2 c) UF-3 d) UF-4 e) UF-5.

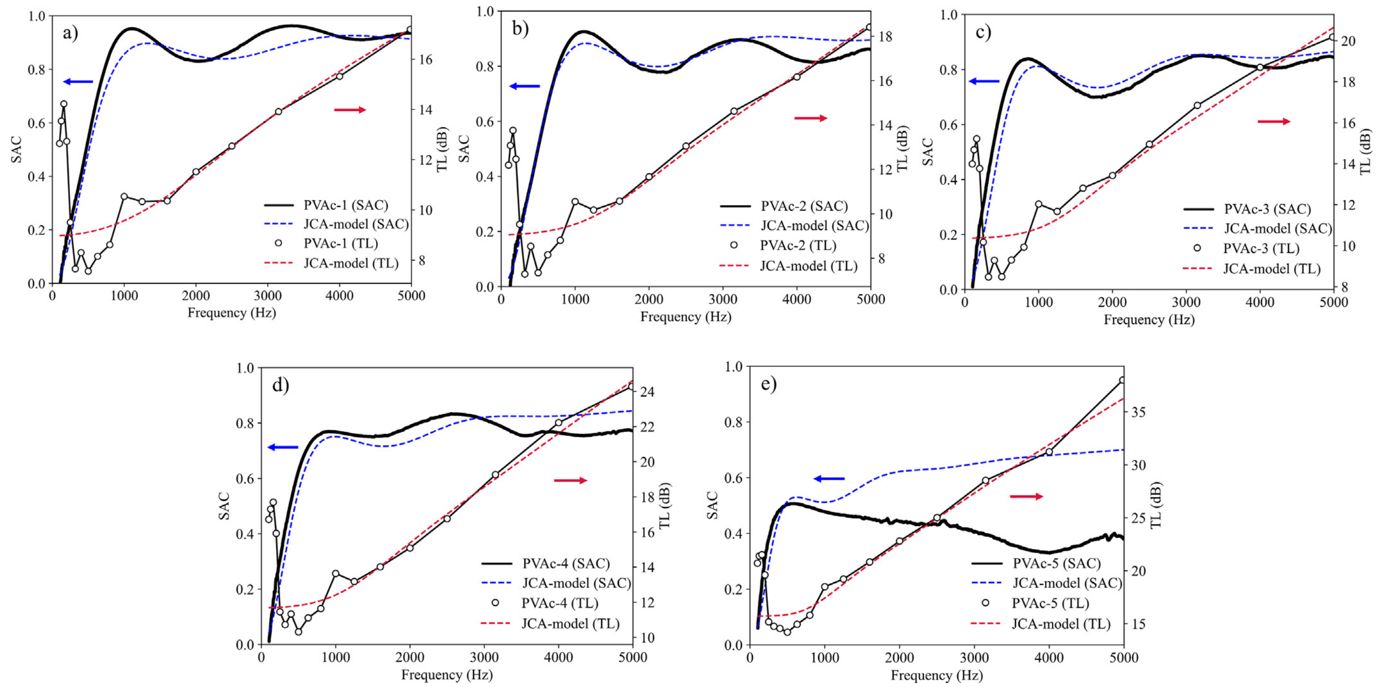

Fig. 12. The experimental sound absorption coefficient (black solid line) and transmission loss (black opened circle) spectra and the least-square fitting of Johnson-Champoux-Allard (JCA) equivalent fluid model (blue and red dashed line for SAC and TL, respectively) a) PVAc-1 b) PVAc-2 c) PVAc-3 d) PVAc-4 e) PVAc-5.

Table 3
The average absolue differences ($\overline{\Delta}_{abs(SAC)}$, and $\overline{\Delta}_{abs(TL)}$) between the experiment and JCA model.

Sample	$\overline{\Delta}_{abs(SAC)}$	$\overline{\Delta}_{abs(TL)}$ (dB)
UF-1	0.028	0.512
UF-2	0.030	0.551
UF-3	0.021	0.587
UF-4	0.034	0.625
UF-5	0.046	1.152
PVAc-1	0.040	0.545
PVAc-2	0.024	0.485
PVAc-3	0.033	0.531
PVAc-4	0.049	0.600
PVAc-5	0.200	0.572

4.3. Direct estimation VS the least-square optimization of porosity

Besides the least-square method discussed in the previous subsection, the porosity of the sample can also be directly estimated using the equation mentioned in the earlier studies [16,44].

$$\phi_f = 1 - \frac{\rho_{bulk}}{\rho_f} \tag{17}$$

where ρ_{bulk} denotes the density of the sample, and ρ_f is the density of the PPFF. Since PPFF is a type of natural fiber, its density is uncertain. In this study, the measured value of ρ_f is varied in between 670–998 kg/m^3.

In this study, there are two components in the samples, including the PPFF and the adhesive. We assumed that the adhesive coats the surface of the fiber resulting in changes in apparent fiber density. To directly estimate the porosity, it is appropriated to consider the adhesive-coated fiber density (ρ_{fa}) instead of the fiber density (ρ_f) alone. Since Ehsan et al. [14] have studied the acoustic property of the composites consisting of two components, we modified their equation to calculate the ρ_{fa} which is the result of the weighted average density between PPFF and the adhesive. ρ_{fa} can be estimated as follows:

$$\rho_{fa} = \frac{\rho_f m_f + \rho_a m_a}{m_f + m_a} \tag{18}$$

where ρ_a is the density the adhesive (1282 kg/m^3 and 1190 kg/m^3 for UF and PVAc, respectively). m_f and m_a are the mass ratios of the PPFF and the adhesives presented in Table 1. Finally, the porosity of the composites consisting of adhesive-coated fiber (ϕ_{fa}) can be calculated as:

Table 4
Optimized Non-acoustical parameters obtained from the least-square fitting of the experimental SAC and TL spectra and Johnson-Champoux-Allard (JCA) model.

Sample	σ (Pa.s.m^{-2})	ϕ	α_∞	Λ (μm)	Λ' (μm)
UF-1	29800 (39)	0.7794 (0.0001)	1.140 (0.010)	39.9 (0.6)	92.6 (0.4)
UF-2	38530 (41)	0.7607 (0.0001)	1.157 (0.001)	31.2 (0.2)	82.9 (0.4)
UF-3	52294 (78)	0.7334 (0.0002)	1.178 (0.001)	18.3(0.7)	19.0 (2.0)
UF-4	74806 (66)	0.7089 (0.0001)	1.205 (0.001)	14.8 (0.3)	41.5 (0.9)
UF-5	112202 (120)	0.6752 (0.0001)	1.241 (0.001)	10.1 (0.9)	11.0 (2.0)
PVAc-1	37000 (42)	0.7637 (0.0001)	1.155 (0.030)	32.0 (0.8)	80.3 (0.5)
PVAc-2	37576 (34)	0.7626 (0.0001)	1.156 (0.030)	30.8 (0.8)	52.0 (2.0)
PVAc-3	46999 (50)	0.7476 (0.0001)	1.171 (0.001)	22.4 (0.4)	22.8 (0.9)
PVAc-4	58087 (71)	0.7292 (0.0001)	1.186 (0.001)	21.0 (0.4)	57.0 (2.0)
PVAc-5	104263 (113)	0.6814 (0.0001)	1.230 (0.060)	9.7 (0.2)	23.7 (0.6)

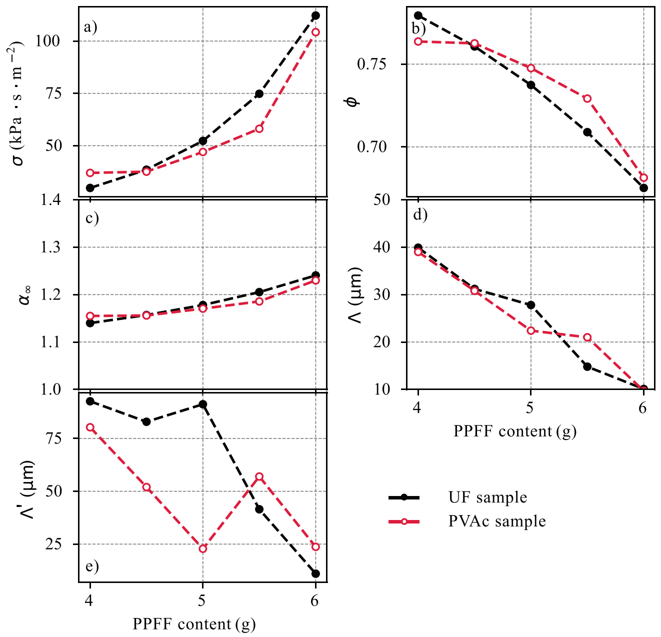

Fig. 13. Non-acoustic parameters of JCA model as variations of sample PPFF content a) airflow resistivity (σ) b) porosity (ϕ) c) tortuosity (α_∞) d) viscous characteristic length (Λ) e) thermal characteristic length (Λ').

$$\phi_{fa} = 1 - \frac{\rho_{bulk}}{\rho_{fa}} \tag{19}$$

The direct estimation of the porosity (ϕ_f and ϕ_{fa}) is shown in Table 5.

From Fig. 14, since ϕ_f (blue color) has been calculated regardless of adhesive effects, the PPFF samples with different adhesives should exhibit no difference. On the other hand, the values of ϕ_{fa} (red color) show the separation between the estimated porosity of samples with UF and PVAc adhesives. It is because the quantity and density of the adhesive play significant roles in determining this value. $\phi_{(JCA)}$ (black color) obtained from the least-square fitting demonstrate similar characteristics with ϕ_{fa}. The average ϕ_{fa} and $\phi_{(JCA)}$ of PVAc samples are collectively higher than UF samples by 2.1 % and 0.73 %, respectively. Furthermore, the coherence between ϕ_{fa} and $\phi_{(JCA)}$, according to Fig. 14, helps verify the reliability of the least-square optimization method used in this study.

This is inferred that the quantity (m_a) and density (ρ_a) of the adhesive contribute to the value of porosity of the PPFF composites. Since all non-acoustic parameters are correlated, the changes

Table 5
The porosity values estimated from the direct estimation methods (Eq. 17ϕ_f), and 19 (ϕ_{fa})) and the least-square method (ϕ_{JCA}) from Table 4

Sample	ϕ_f	ϕ_{fa}	ϕ_{JCA}
UF-1	0.691	0.763	0.7794
UF-2	0.655	0.732	0.7607
UF-3	0.650	0.724	0.7334
UF-4	0.613	0.692	0.7089
UF-5	0.595	0.674	0.6752
PVAc-1	0.713	0.754	0.7637
PVAc-2	0.711	0.750	0.7626
PVAc-3	0.707	0.743	0.7476
PVAc-4	0.690	0.727	0.7292
PVAc-5	0.648	0.687	0.6814

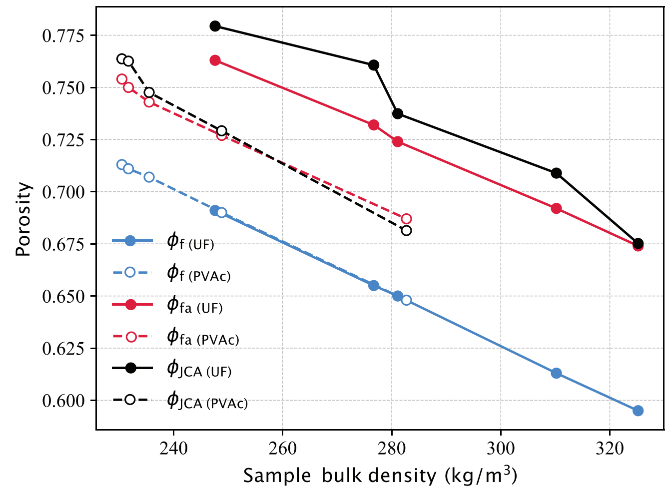

Fig. 14. The porosity of the samples estimated from various methods including the direct calculation from Eq. 17 (blue), Eq. 19 (red), and the least-square optimization using JC.A model (black).

in porosity will ultimately result in changes in material acoustic properties. By manipulating the quantity and density of an adhesive according to Eq. 17 and Eq. 19, researchers can control and predict the outcome of the SAC and TL of the designed fibrous sound absorbers via the JCA model or other empirical estimations that will be developed in the future.

5. Conclusion

As an alternative to conventional synthetic fibers, palmyra palm fruit fiber (PPFF) has advantages, including sustainability, recyclability, renewability, and abundance. This work examined and investigated the acoustic properties of PPFF composites combined with UF and PVAc adhesive using experimental and computational methods. The conclusion can be written as follows:

- The normal-incident sound absorption coefficient (SAC) spectra are higher in the samples with lower PPFF contents. The PPFF composites could be a promising sound absorber with the highest NRC of 0.63.
- It is the opposite for the transmission loss (TL), where samples with higher PPFF contents show higher TL spectra. The highest TL_{5000} is 37.8 dB.
- The least-square fitting of the Johnson-Champoux-Allard (JCA) equivalent fluid model is consistent with the experimental SAC and TL results for most samples. The optimized airflow resistivity (σ) and the tortuosity (α_∞) show the direct variation with the PPFF content. On the other hand, the porosity (ϕ), viscous characteristic length (Λ), and thermal characteristic length (Λ') demonstrate inverse variation with the PPFF content.
- The optimized porosity values obtained from the JCA model (ϕ_{JCA}) are coherent with those from the direct estimation method assuming adhesive-coated fiber (ϕ_{fa}). This is inferred that the adhesive's quantity and density contribute to the composites' porosity value, ultimately affecting material acoustic properties. Researchers can control and predict how the SAC and TL of specially engineered fibrous sound absorbers would behave by varying the quantity and density of an adhesive.
- The direct measurement of airflow resistivity to make an empirical acoustic model for PPFF composites and the application of more recent semi-phenomenological models [28,27,45] are worth being investigated in the future.

CRediT authorship contribution statement

Purintorn Chanlert: Conceptualization, Methodology, Software, Validation, Formal analysis, Investigation, Resources, Data curation, Writing - original draft, Writing - review & editing, Visualization, Supervision, Project administration, Funding acquisition. **Sukrutai Tongyoo:** Validation, Investigation, Resources, Writing - review & editing. **Chintaporn Rordrak:** Validation, Investigation, Resources, Writing - review & editing.

Declaration of Competing Interest

The authors declare that they have no known competing financial interests or personal relationships that could have appeared to influence the work reported in this paper.

Acknowledgement

The authors appreciate the Faculty of Science and Technology, Songkhla Rajabhat University, for providing the equipment and facilities necessary for this study.

References

[1] Aso S, Kinoshita R. Sound absorption coefficient of glass wool. J Textile Mach Soc Jpn - Trans 1965;18:T649–53.
[2] Uris A, Llopis A, Llinares J. Effect of the rockwool bulk density on the airborne sound insulation of lightweight double walls. Appl Acoust 1999;58:327–31.
[3] Yang Y, Li B, Chen Z, Sui N, Chen Z, Xu T, Li Y, Fu R, Jing Y. Sound insulation of multi-layer glass-fiber felts: Role of morphology. Text Res J 2017;87:261–9.
[4] Itewi M. Green building construction thermal isolation materials (Rockwool). Am J Environ Sci 2011;7:161–5.
[5] Kudo Y, Kotani M, Tomita M, Aizawa Y. Effects of rock wool on the lungs evaluated by magnetometry and biopersistence test. J Occupational Med Toxicol 2009;4:1–7.
[6] Koizumi T, Tsujiuchi N, Adachi A. The development of sound absorbing materials using natural bamboo fibers, High Performance. Struct Mater 2002;4:157–66.
[7] Yang H-S, Kim D-J, Kim H-J. Rice straw-wood particle composite for sound absorbing. Bioresour Technol 2003;86:117–21.
[8] Zulkifli R, Mohd Nor MJ, Mat Tahir MF, Ismail AR, Nuawi MZ. Acoustic properties of multi-layer coir fibres sound absorption panel. J Appl Sci 2008;8:3709–14.
[9] Hosseini Fouladi M, Nor MJM, Ayub M, Leman ZA. Utilization of coir fiber in multilayer acoustic absorption panel. Appl Acoust 2010;71:241–9.
[10] Kang CW, Oh SW, Lee TB, Kang W, Matsumura J. Sound absorption capability and mechanical properties of a composite rice hull and sawdust board. J Wood Sci 2012;58:273–8.
[11] Taban E, Valipour F, Abdi DD, Amininasab S. Mathematical and experimental investigation of sound absorption behavior of sustainable kenaf fiber at low frequency. Int J Environ Sci Technol 2020;18:2765–80.
[12] Delany ME, Bazley EN. Acoustical properties of fibrous absorbent materials. Appl Acoust 1970;3:105–16.
[13] Berardi U, Iannace G. Predicting the sound absorption of natural materials: Best-fit inverse laws for the acoustic impedance and the propagation constant. Appl Acoust 2017;115:131–8.
[14] Ehsan Samaei S, Berardi U, Taban E, Soltani P, Mohammad Mousavi S. Natural fibro-granular composite as a novel sustainable sound-absorbing material. Appl Acoust 2021;181:108157.
[15] Abdi DD, Monazzam M, Taban E, Putra A, Golbabaei F, Khadem M. Sound absorption performance of natural fiber composite from chrome shave and coffee silver skin. Appl Acoust 2021;182:108264.
[16] Taban E, Amininasab S, Soltani P, Berardi U, Abdi DD, Samaei SE. Use of date palm waste fibers as sound absorption material. J Building Eng 2021;41:102752.
[17] Shahrzad M, Ebrahim T, Parham S, Seyed Ehsan S, Ali K. Sugarcane bagasse waste fibers as novel thermal insulation and sound-absorbing materials for application in sustainable buildings. Build Environ 2022;211:108753.
[18] Davis TA, Johnson DV. Current utilization and further development of the palmyra palm (Borassus flabellifer L., Arecaceae) in Tamil Nadu state, India. Econ Bot 1987;41:247–66.
[19] Krishnaveni TRS, Arunachalam R, Chandrakumar M, Parthasarathi G, Nisha R. Potential Review on Palmyra (Borassus flabellifer L). Adva Res 2020;21:29–40.
[20] Johnson DL, Koplik J, Dashen R. Theory of dynamic permeability and tortuosity in fluid saturated porous media. J Fluid Mech 1987;176:379–402.
[21] Allard JF, Champoux Y, New empirical equation for sound propagation in rigid frame fibrous materials (1992) 3346–3353.
[22] Schneider CA, Rasband WS, Eliceiri KW. NIH Image to ImageJ: 25 years of image analysis. Nat Methods 2012;9:671–5.
[23] ASTM-E1050, Standard test method for impedance and absorption of acoustical materials using a tube, two microphones and a digital frequency analysis system, 1990.
[24] ISO-10534, Determination of sound absorption coefficient and impedance in impedance tubes: Part 2: Transfer-function method, 1998.
[25] Koruk H. An assessment of the performance of impedance tube method. Noise Control Eng J 2014;62:264–74.
[26] ASTM-E2611, Standard Test Method for Normal Incidence Determination of Porous Material Acoustical Properties Based on the Transfer Matrix Method, 2019.
[27] Pride SR, Morgan FD, Gangi AF. Drag forces of porous-medium acoustics. Phys Rev B 1993;47:4964–78.
[28] Lafarge D, Lemarinier P, Allard JF, Tarnow V. Dynamic compressibility of air in porous structures at audible frequencies. J Acoust Soc Am 1997;102:1995–2006.
[29] Allard JF, Atalla N. Propagation of Sound in Porous Media. 1st ed. Hoboken, New Jersey, USA: Wiley; 2009.
[30] Bonfiglio P, Pompoli F. Inversion problems for determining physical parameters of porous materials: Overview and comparison between different methods. Acta Acustica united with Acustica 2013;99:341–51.
[31] Nennig B, Binois R, Dauchez N, Perrey-Debain E, Foucart F. A transverse isotropic equivalent fluid model combining both limp and rigid frame behaviors for fibrous materials. J Acoust Soc Am 2018;143:2089–98.
[32] Jiménez N, Romero-García V, Groby JP. Perfect absorption of sound by rigidly-backed high-porous materials. Acta Acustica united with Acustica 2018;104:396–409.
[33] Magliacano D, Ouisse M, Khelif A, De Rosa S, Franco F, Atalla N, Collet M. Computation of dispersion diagrams for periodic porous materials modeled as equivalent fluids. Mech Syst Signal Process 2020;142:106749.
[34] Luu HT, Perrot C, Panneton R. Influence of porosity, fiber radius and fiber orientation on the transport and acoustic properties of random fiber structures. Acta Acustica united with Acustica 2017;103:1050–63.
[35] Liu Z, Zhan J, Fard M, Davy JL. Acoustic properties of multilayer sound absorbers with a 3D printed micro-perforated panel. Appl Acoust 2017;121:25–32.
[36] Newville A, Matthew; Stensitzki, Till; Allen, Daniel B.; Ingargiola, Python, LMFIT: Non-Linear Least-Square Minimization and Curve-Fitting for, 2014. doi: 10.5281/zenodo.11813.
[37] Carman PG. Fluid flow through granular beds. Chem Eng Res Des 1997;75: S32–48.
[38] Pelegrinis MT, Horoshenkov KV, Burnett A. An application of Kozeny-Carman flow resistivity model to predict the acoustical properties of polyester fibre. Appl Acoust 2016;101:1–4.
[39] Berryman JG. Confirmation of Biot's theory. Appl Phys Lett 1980;37:382–4.
[40] Raj M, Fatima S, Tandon N. Recycled materials as a potential replacement to synthetic sound absorbers: A study on denim shoddy and waste jute fibers. Appl Acoust 2020;159.
[41] ISO-11654, Acoustics – sound absorbers for use in buildings – rating of sound absorption., 1997.
[42] Neri M, Levi E, Cuerva E, Pardo-Bosch F, Zabaleta AG, Pujadas P. Sound absorbing and insulating low-cost panels from end-of-life household materials for the development of vulnerable contexts in circular economy perspective. Appl Sci (Switzerland) 2021;11:1–19.
[43] Norton MP, Karczub DG, Fundamentals of noise and vibration analysis for engineers, 2nd Edition, 2nd ed., 2003. doi: 10.3397/1.2721371.
[44] Soltani P, Taban E, Faridan M, Samaei SE, Amininasab S. Experimental and computational investigation of sound absorption performance of sustainable porous material: Yucca Gloriosa fiber. Appl Acoust 2020;157:106999.
[45] Horoshenkov KV, Groby J-P, Dazel O. Asymptotic limits of some models for sound propagation in porous media and the assignment of the pore characteristic lengths. J Acoust Soc Am 2016;139:2463–74.
[46] Bansod PV, Mohanty AR. Inverse acoustical characterization of natural jute sound absorbing material by the particle swarm optimization method. Appl Acoust 2016;112:41–52.